Icarus 243 (2014) 129–138

Contents lists available at ScienceDirect

Icarus

journal homepage: www.elsevier.com/locate/icarus

Subsidence-induced methane clouds in Titan's winter polar stratosphere and upper troposphere

C.M. Anderson [a,*], R.E. Samuelson [b], R.K. Achterberg [b], J.W. Barnes [c], F.M. Flasar [a]

[a] Planetary Systems Laboratory, NASA Goddard Space Flight Center, Greenbelt, MD 20771-0001, USA
[b] Department of Astronomy, University of Maryland, College Park, MD 20742-2421, USA
[c] Department of Physics, University of Idaho, Moscow, ID 83844-0903, USA

ARTICLE INFO

Article history:
Received 30 July 2013
Revised 4 September 2014
Accepted 4 September 2014
Available online 16 September 2014

Keywords:
Titan, clouds
Atmosphere
Radiative transfer
Ices, IR spectroscopy

ABSTRACT

Titan's atmospheric methane most likely originates from lakes at the surface and subsurface reservoirs. Accordingly, it has been commonly assumed that Titan's tropopause region, where the vertical temperature profile is a minimum, acts as a cold trap for convecting methane, leading to the expectation that the formation of methane clouds in Titan's stratosphere would be rare. The additional assumption that Titan's tropopause temperatures are independent of latitude is also required. However, Cassini Composite InfraRed Spectrometer (CIRS) and Radio Science Subsystem (RSS) data sets reveal colder temperatures in Titan's tropopause region near the winter pole than those at low latitudes and in the summer hemisphere. This, combined with the presence of a cross-equatorial meridional circulation with winter polar subsidence, as suggested by current general circulation models, implies the inevitable formation of Subsidence-Induced Methane Clouds (SIMCs) over Titan's winter pole. We verified this by retrieving the stratospheric methane mole fraction at 70°N from the strength of the far infrared methane pure rotation lines observed by CIRS and by assuming the RSS-derived thermal profile at 74.1°N. Our retrieved methane mole fraction of 1.50 ± 0.15% allows for methane to condense and form SIMCs at altitudes between ~48 and ~20 km. Radiative transfer analyses of a color composite image obtained by the Cassini Visible and Infrared Mapping Spectrometer (VIMS) during northern winter appear to corroborate the existence of these clouds.

Published by Elsevier Inc.

1. Introduction

There are two distinct types of cloud systems in Titan's atmosphere. The first and more familiar type consists of convective methane clouds produced in the troposphere. As with water on Earth, methane has a source at Titan's surface, and therefore the methane cycle on Titan has been presumed akin to that of Earth's convective water cycle in which phase changes are confined to the troposphere. During southern summer on Titan, the surface is heated at mid to high southern latitudes, which drives turbulent upwelling (convection). This results in the formation of methane cloud particles that grow large quickly and then fall out of the atmosphere on time scales from hours to days (see for example Griffith et al., 2005). Starting in early southern summer on Titan, ground-based images revealed convective methane clouds located predominantly poleward of 70°S (e.g. Roe et al., 2002). As southern summer progressed, with the arrival of the Cassini Spacecraft in the Saturn system, clouds at mid and low southern latitudes became observable (e.g. Porco et al., 2005). As Titan moved into late northern winter, and then into early northern spring, the high southern latitude clouds essentially vanished (Rodriguez et al., 2011), the mid southern latitude clouds endured, and equatorial, and then mid and high northern latitude convective clouds began to emerge (e.g. Turtle et al., 2011). Thus, Titan's convective methane cloud systems tend to follow the Sun as it migrates with season.

The second type of cloud system is the direct result of Titan's overall atmospheric circulation pattern. Because Titan is a slow rotator, latitudinal heat and momentum transport is accomplished mainly through slow, axially symmetric meridional circulation (Leovy and Pollack, 1973; Flasar et al., 1981). General circulation models (GCMs) that do not include such processes as moist convection, for example, predict only a single cell during northern winter. Circulation is from north to south near the surface, and from south to north in the stratosphere and mesosphere, with upwelling at mid to high southern latitudes and subsidence at mid to high northern latitudes (e.g. Lebonnois et al., 2012, and references therein). This slow, axisymmetric meridional circulation

* Corresponding author.

http://dx.doi.org/10.1016/j.icarus.2014.09.007
0019-1035/Published by Elsevier Inc.

is responsible for cloud formation in the mid to lower stratosphere. Most organic vapors are produced in Titan's mesosphere and above, and are abundant enough to partially condense as they are transported downward to cooler temperatures, forming Titan's second type of cloud system — subsidence-induced clouds in the winter polar stratosphere. These clouds are relatively stable, long-lived, and tend to have particles with effective radii between 1 and 5 μm. Observed examples include those of condensed dicyanoacetylene (C_4N_2: Khanna et al., 1987; Samuelson et al., 1997a), cyanoacetylene (HC_3N: Anderson et al., 2010), hydrogen cyanide (HCN: Samuelson et al., 2007), blended HCN and HC_3N (Anderson and Samuelson, 2011), and ethane (C_2H_6: Mayo and Samuelson, 2005; Griffith et al., 2006; Anderson and Samuelson, 2011).

Of the various volatile gases, methane vapor provides the major exception. Its source is at the surface, and Titan's meridional circulation pattern by itself will not give rise to methane condensation in the stratosphere as long as tropopause temperatures are roughly constant with latitude. Indeed, both Flasar et al. (1981) and Samuelson et al. (1997b) analyzed Voyager 1 InfraRed Interferometer Spectrometer (IRIS) data and found little tropopause temperature variation between latitudes ±60°. However, Cassini's Composite InfraRed Spectrometer (CIRS) and Radio Science Subsystem (RSS) instruments enable us to determine tropopause temperatures at much higher latitudes (for retrieval procedures see Anderson and Samuelson, 2011; Schinder et al., 2011, 2012). In particular, both instruments indicate tropopause temperatures several kelvins cooler at very high northern latitudes compared with those at lower latitudes, including the 70.43 ± 0.25 K measured value at 10°S by the Huygens Atmospheric Structure Instrument (HASI; Fulchignoni et al., 2005). As we show in the following sections, cooler tropopause temperatures, when coupled with the expected axisymmetric circulation pattern, lead to the formation of Subsidence-Induced Methane Clouds (hereafter SIMCs) in Titan's north polar stratosphere and upper troposphere. We demonstrate that for latitudes poleward of ~65°N, methane ice can, and in fact probably does, comprise much of Titan's northern winter polar cloud discovered by Cassini's Visible and Infrared Mapping Spectrometer (VIMS; Griffith et al., 2006). We discuss the physical processes involved in the formation of SIMCs in Section 2, followed by a determination of the stratospheric CH_4 mole fraction at 70°N in Section 3. We infer temperatures surrounding the tropopause from CIRS data at 85°N in Section 4, and ramifications and results in Section 5. We then provide evidence of SIMCs from VIMS data in Section 6. A synopsis and short discussion are given in Section 7.

2. Physical rationale behind SIMCs

The presence of a long-lived condensation cloud in Titan's stratosphere depends on two requirements: (1) the given volatile must be supersaturated at the ambient temperature, and, (2) as the resulting condensate is removed from a given locale by advection or precipitation, the magnitude of the replacement flux of volatile vapor must be adequate for maintaining the cloud. This flux depends strongly on Titan's atmospheric axially symmetric meridional circulation pattern. The simplified pattern during northern winter solstice that we consider is illustrated in Fig. 1.

In the stratosphere, the downward flux component is the important one, because it transports vapor from warmer regions to colder ones, enabling condensation. The circulation scenario depicted in Fig. 1 implies that very little downward flux of vapor at low latitudes is due to meridional circulation. Any downward flux of vapor there is more likely due to eddy diffusion, which is not very effective in general. The much stronger downward flux due to subsidence is likely to occur only at high northern (winter) latitudes.

Thus vapors originating at high altitudes (this includes all the trace organics) will in all likelihood condense in the mid to lower stratosphere, preferentially at high winter latitudes. Although some condensation may take place in the stratosphere at low latitudes, the associated small downward flux component ensures

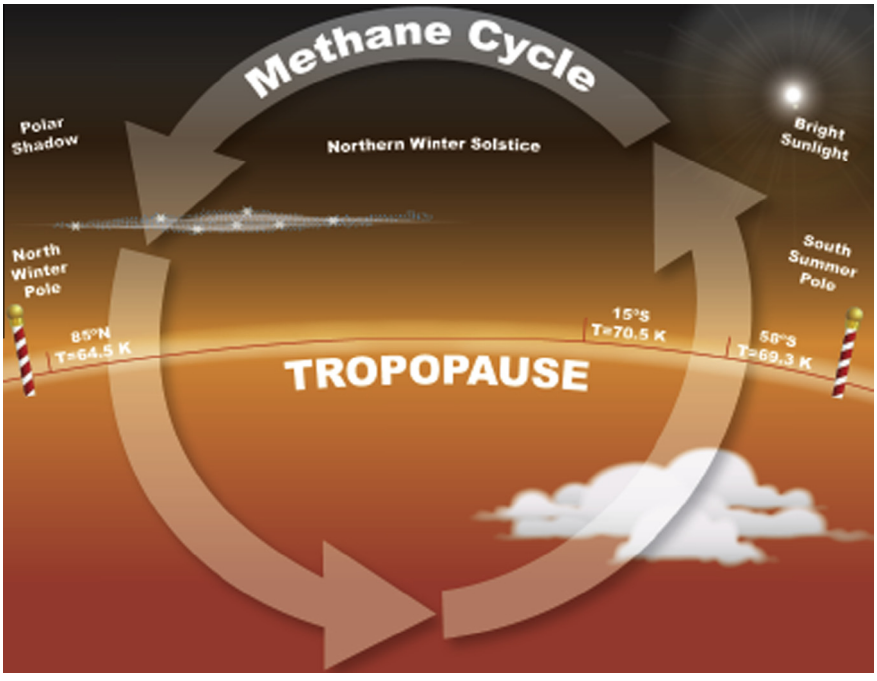

Fig. 1. Schematic illustrating Titan's meridional circulation pattern expected during northern winter. In the south, methane vapor pushes through Titan's cold trap into the stratosphere and then moves along stream lines in the stratosphere and mesosphere to high northern latitudes where subsidence occurs. CIRS and RSS show much colder tropopause temperatures at high northern latitudes, leading to methane condensation there via subsidence in the lower stratosphere and upper troposphere. Image Credit: Jay Friedlander.

that the optical thickness of any resulting steady-state cloud will be relatively small. This is probably the reason that diffuse ethane clouds, for example, have been observed by VIMS only near the north winter pole (Griffith et al., 2006), where strong subsidence occurs. Even though some condensation of ethane probably occurs at low latitudes in the stratosphere, the resulting steady-state cloud formation is optically too thin to be observed.

In the case of methane, the source is at the surface. Upward transport of methane vapor through Titan's cold trap, located just below the relatively warmer southern tropopause, enables a certain fraction of methane vapor to enter the lower stratosphere at southern latitudes. Due to the lack of significant known sources or sinks of methane vapor in Titan's stratosphere, this methane mole fraction might be expected to remain essentially constant as methane is circulated to high northern latitudes, where the methane vapor then subsides and some of it condenses. According to measurements from the Huygens Gas Chromatograph/Mass Spectrometer (GCMS), the stratospheric mole fraction q(CH_4) is 1.48 ± 0.09% at 10°S (Niemann et al., 2010). However, a recent analysis of CIRS data at 15°S by Lellouch et al. (2014) suggests a much lower value of q(CH_4), ~0.95 ± 0.08%. Generally, Lellouch et al. (2014) found q(CH_4) values near 1.0% at lower latitudes and near ±50–55° and q(CH_4) values near 1.5% at ±30–35° and polar latitudes (except at 70°N where they retrieve a methane mole fraction value of 1.08%).

The stratospheric methane mole fractions at 62°N and 70°N that were deduced by Lellouch et al. (2014) are quite dissimilar; this is unexpected for latitudes so close together. On the other hand, these two latitudes are the ones for which the methane mole fraction needs to be known with precision in order to determine whether or not methane condensation due to subsidence will occur. We therefore devote considerable effort in assessing whether these two methane mole fractions can be reconciled. We restrict our quantitative analysis to 70°N where we have available a temperature profile determined solely (and independently) from RSS occultation data.

3. Stratospheric methane mole fraction at 70°N

In order to establish the likelihood of methane condensing in or near Titan's winter polar lower stratosphere, we need to accomplish two tasks. The first task is to determine actual temperatures in the altitude region spanning Titan's tropopause at high winter latitudes. The second task is to determine the methane mole fraction just above this region. Because of its critical importance and controversial nature, we will discuss this latter task at considerable length.

We defer a discussion of tropopause temperatures to Sections 4 and 5, and restrict this section to an examination of the stratospheric methane abundance at high northern latitudes. According to Lellouch et al. (2014), the stratospheric methane mole fraction q(CH_4) is ~1.49 ± 0.16% at 62°N, but drops precipitously to ~1.08 ± 0.21% at 70°N. This latter mole fraction may be too low to support methane condensation in the lower stratosphere, so we need to examine its determination more closely.

3.1. RSS temperature profile – comparison with CIRS from Lellouch et al. (2014)

Crucial to any radiative transfer retrieval of q(CH_4) from the pure methane rotation lines between ~70 and 165 cm^{-1} (as Lellouch et al., 2014, have done), is the temperature profile used in the analysis. Lellouch et al. (2014) use a constrained linear inversion procedure to infer Titan's temperature profile at 70°N from CIRS spectra acquired at that latitude. Results are shown by the pink curve in Fig. 2. The mean tangent height associated with the CIRS limb integration spectrum (from which the results were derived) is 147 km. According to Lellouch et al. (2014), the pressure ranges color-coded in yellow in Fig. 2 are those over which temperatures can be inferred directly from the 147 km limb data. The derived temperature profile at 70°N is shown by solid pink curve segments over these ranges. Outside these pressure ranges little direct temperature information is available from CIRS, and the temperature profile is a result of interpolation, extrapolation, or relaxation to the initial starting (*a priori*) temperature profile. Temperatures over these latter ranges are indicated in Fig. 2 by dotted pink curve segments; these ranges are also defined by the white regions in the figure.

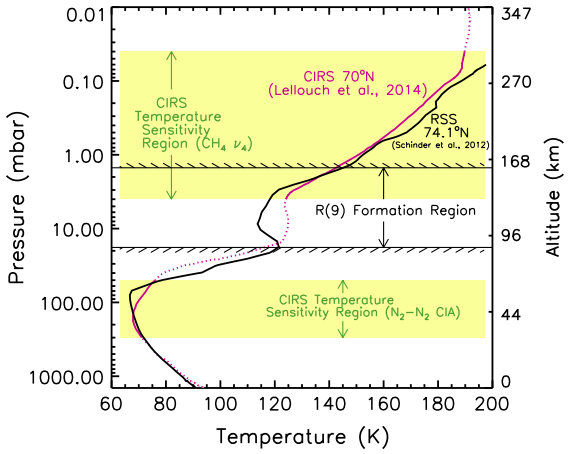

Fig. 2. Temperature–pressure–altitude diagram at 70°N from CIRS (pink curve; Lellouch et al., 2014) and at 74.1°N from RSS (black curve; Schinder et al., 2012). The solid pink curve segments and the yellow color-coded rectangles represent pressure–altitude regions where CIRS has temperature information from the CH_4 ν_4 band at 7.7 μm (top yellow region) and from the far-IR continuum opacity between 70 and 140 cm^{-1} resulting mainly from N_2–N_2 CIA, with non-negligible contributions from aerosol and stratospheric nitrile ices (lower yellow region). The dotted pink curve segments in the white regions refer to pressure ranges over which temperature information that is directly derivable from CIRS spectra is minimal. The thin hatched black lines at 1.5 and 18 mbar are boundaries of the pressure range over which the CH_4 R(9) pure rotation line at 104.25 cm^{-1} is dominantly formed. (For interpretation of the references to color in this figure legend, the reader is referred to the web version of this article.)

We need to determine the altitude region over which the methane rotation lines are formed at 70°N. Although Lellouch et al. (2014) do not compute methane rotation line contribution functions for CIRS data at 70°N, they do compute them for 62°N under very similar limb-tangent viewing conditions. The two data sets are for northern winter conditions and are close in latitude, suggesting that contribution functions should be similar in the two data sets. The thin, hatched black lines at 1.5 and 18 mbar in Fig. 2 denote the pressures at which the half-power points of the contribution function for the methane R(9) rotation line at 104.25 cm^{-1} (highest signal-to-noise rotation line for CIRS), as calculated by Lellouch et al. (2014), are located. These boundaries should therefore define approximately the pressure range over which the pure methane rotation lines between 70 and 165 cm^{-1} are formed.

According to Fig. 2, the pressure ranges over which the methane rotation lines are formed, and where temperatures cannot be determined directly from CIRS data, show considerable overlap. This suggests that it is extremely difficult to infer methane mole fractions at 70°N from CIRS data alone. Fortunately, a nearby wintertime RSS radio occultation temperature profile, acquired during the T31 flyby on 28 May 2007, is available at 74.1°N (Schinder et al., 2012). This profile does not suffer from the restrictions

associated with CIRS-related temperature determinations. The RSS profile is shown by the black curve in Fig. 2.

Large differences between the CIRS and RSS temperature profiles at 70°N are apparent between about 4 and 12 mbar, where the RSS temperatures range between ~6 and 11 K lower than those inferred from CIRS. This pressure range also corresponds closely both to the region of maximum rotation line formation and to the region where direct temperature information is not available from CIRS data. We therefore adopt the RSS temperature profile and use it to determine the methane mole fraction from the rotation line strengths associated with the CIRS limb integration spectrum at 70°N (even though the RSS temperature information is strictly valid only at 74.1°N).

3.2. Opacity contributors to the spectral continuum

The methane rotation line strengths between 70 and 165 cm^{-1} are measured relative to the adjacent continuum. The continuum itself is formed mainly from three sources of opacity: N_2–N_2 collision-induced absorption (CIA), a photochemically-produced aerosol, and a spectroscopically broad ice feature, identified by Anderson and Samuelson (2011) as arising from lattice vibrations of a combination of nitrile ices, notably those of HCN and HC_3N. N_2–CH_4 CIA is too weak to contribute between 70 and 165 cm^{-1}. Although the relatively narrow nitrile ice cloud tends to form near the bottom of the region of methane rotation line formation at low latitudes, vapor abundances of HCN and HC_3N are much greater at high northern (winter) latitudes, and the cloud forms higher up, near the middle of the line formation region (see Fig. 2). On the other hand, the aerosol is spread diffusely throughout the entire vertical range over which CIRS is sensitive. The aerosol scale height is somewhat variable, averaging out to be about 1.7 times the pressure scale height, as determined at 15°S by Anderson and Samuelson (2011).

Thus opacities due to both cloud and aerosol contribute to a foreground continuum that partially obscures the methane rotation lines, thereby reducing their observed strengths. As a result, it is necessary to infer the vertical distributions of particulate opacities in order to derive precise methane mole fractions.

A procedure for doing this from FP1 CIRS scans across Titan's limb was developed by Anderson and Samuelson (2011). FP1 is the focal plane covering the 10–600 cm^{-1} spectral region, and its 6.4 mrad circular field of view (FOV) subtends a vertical tangent height range ~200 km during a typical limb scan. However, there is roughly 99% overlap between contiguous FOVs during a scan. This enables not only a retrieval at each wavenumber of the intensity integrated over the FOV, but also a retrieval of the derivative of this integral, i.e., the intensity itself as a function of tangent height. Thus, for sufficiently high signal-to-noise, the geometric thickness δz of a nitrile cloud layer can be determined from limb scans even if δz is several times smaller than the FOV diameter.

Anderson and Samuelson (2011) derived the spectral variations and the vertical distributions separately for both the aerosol and the nitrile ice cloud at three latitudes: 15°N, 15°S, and 58°S. They found little latitudinal variation in the *spectral characteristics* of both aerosol and ice, implying the chemical compositions of both are largely independent of latitude.

We apply these results to the task of determining continuum characteristics of limb integration spectra at other latitudes. We choose as a test case the CIRS limb integration spectrum at 62°N, mainly because it is the best example we could find that illustrates the strong need for all three continuum components: aerosol, nitrile ice, and N_2–N_2 CIA. It is also associated with the critically important high northern latitude region.

The spectrum is shown in Fig. 3. It consists of an average of 24 individual spectra, covering the FP1 wavenumber range

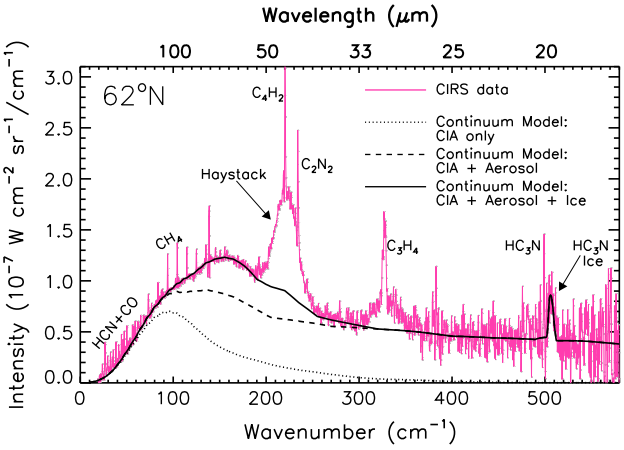

Fig. 3. CIRS far-IR limb integration spectrum of Titan at 0.48 cm^{-1} spectral resolution acquired at 62°N at a limb tangent height of ~125 km during the T15 Titan flyby (solid pink curve). Various organic vapors and the Haystack (broad 220 cm^{-1} ice cloud feature) are labeled. The dotted, dashed, and solid black curves are respectively synthetic spectra of our continuum model: (1) with CIA only, (2) with CIA and aerosol, and (3) with CIA, aerosol, and ice. (For interpretation of the references to color in this figure legend, the reader is referred to the web version of this article.)

10–600 cm^{-1}. The center of the FP1 FOV is located at a tangent height of ~125 km above Titan's surface. Below 160 km at 62°N, no reliable temperature data can be inferred from CIRS spectra (except the region surrounding the tropopause). We therefore take an average of 53°N and 74°N from the RSS profiles (Schinder et al., 2012) to represent the *a priori* temperature structure below 160 km. Above 160 km, the temperature profile at 62°N is derived from the CIRS CH_4 ν_4 band using a constrained linear inversion technique (Achterberg et al., 2008).

We initially adopt the spectral dependences and vertical distributions of aerosol and nitrile ice that we derived at 15°N. We then raised the ice cloud from ~85 km to ~143 km, since HCN and HC_3N saturate respectively at 141 km and 145 km for the 62°N vapor abundances derived by Coustenis et al. (2007). Adjustments to the aerosol and nitrile ice abundances are found by iteration. Our best fit continuum model requires no aerosol scale factor, an ice scale factor of 0.5, and a vertical offset of −1.0 km to the data. Results are shown in Fig. 3.

It is immediately apparent from the figure that all three continuum opacity components are important, and that their contributions can be determined separately. The CIA component between 10 and 160 cm^{-1} is due mostly to N_2–N_2 collisions, and is quite strong at ~100 cm^{-1}. The aerosol component is basically responsible for the entire continuum between 300 and 600 cm^{-1}, and, in spite of severe noise, is well determined. The remaining contribution to the continuum opacity is then readily determined by adjusting the magnitude of the nitrile ice opacity. This component peaks at ~160 cm^{-1}.

Fig. 3 indicates that a substantial fraction of the continuum between 70 and 165 cm^{-1} is due to particulate opacity. Some of this opacity will act as a foreground extinction, partially reducing the observed strengths of the methane rotation lines contained in the 70 and 165 cm^{-1} spectral interval. The five strongest rotation lines shown in the figure are R(8) at 93.90 cm^{-1} through R(12) at 135.05 cm^{-1}. Radiative transfer calculations show that adding the particulate opacity systematically reduces line strengths by 12% at R(8) and 21% at R(12). The percentages of these reductions contributed by the nitrile ice cloud range from 33% at R(8) to 44% at R(12); the aerosol therefore contributes respectively 67% and 56% of those reductions at these same lines.

3.3. Procedure for determining the methane mixing ratio at 70°N

The CIRS limb integration spectrum at 70°N was acquired during the T35 Cassini flyby on 31 August 2007, and is the one we used to obtain the methane mole fraction there. In this type of CIRS data acquisition mode, the spectral average is acquired in a limb-integration sequence in which the far-IR FOV is restricted to a closely-grouped set of tangent heights on the limb over a small altitude range. These spectra are recorded at the CIRS highest spectral resolution of 0.48 cm^{-1}, necessary to resolve the methane far-IR rotation lines. The 70°N average spectrum contains 25 individual spectra in which the center of the CIRS far-IR focal plane spans tangent heights 133 to 161 km, with a mean value of 147 km. Just three months prior to the CIRS limb integration, the RSS radio occultation at 74.1°N was recorded during the T31 flyby on 28 May 2007 (Schinder et al., 2012). As indicated in Section 3.1, the temperature profile derived from this occultation (using $q(CH_4) = 1.5\%$) is the *a priori* temperature profile that we used to analyze the CIRS spectrum at 70°N. In practice, each time the stratospheric methane mole fraction was varied in our radiative transfer model, we adjusted the RSS temperature–pressure profile to maintain consistency with the radio occultation data (see Fjeldbo and Eshleman, 1968; Flasar, 1983). Changes in the mean molecular mass and atmospheric refractivity are slight, and the adjustments were small.

The synthetic spectrum at 70°N is computed spanning the wavenumber range 10–600 cm^{-1}. The continuum requires opacity input from seven combinations of N_2–CH_4–H_2 CIA pairs: N_2–N_2, N_2–CH_4, N_2–$H_{2,para}$, N_2–$H_{2,ortho}$, CH_4–$H_{2,para}$, CH_4–$H_{2,ortho}$, and CH_4–CH_4 (Borysow and Frommhold, 1986a,c,b; Borysow and Tang, 1993). We assumed that the relative abundances of $H_{2,ortho}$ and $H_{2,para}$ were compatible with thermodynamic equilibrium at the local temperature. Opacities from the aerosol and the blended HCN–HC_3N lower stratospheric ice cloud were also required. We included an opacity adjustment for N_2–CH_4 CIA as a function of both altitude and wavenumber, following the procedure described in Anderson and Samuelson (2011).

We initially adopted the vertical and spectral dependences of the aerosol and composite nitrile ice cloud derived from our limb scan analysis at 15°N (Anderson and Samuelson, 2011), except for an altitude adjustment of the ice cloud to 143 km. We then ran a forward model iteratively, adjusting the 15°N aerosol opacity to fit the CIRS limb integration spectrum at 70°N between 300 and 600 cm^{-1}. We also included contributions from the stratospheric nitrile ice cloud between ~100 and 260 cm^{-1}. A few small tweaks over the entire spectral range covering 10–600 cm^{-1} was then needed in order to fine tune the ice opacity, aerosol opacity, and N_2–N_2 CIA opacity. Adjustments to the N_2–N_2 CIA opacity were determined by applying a vertical offset to the model.

For the 70°N limb integration spectrum, a vertical offset of −8.5 km was necessary. There was no need to adjust the magnitude of the aerosol opacity compared with that at 15°N, but the ice opacity required a decrease by a factor of 0.29. This reduction factor resulted from a lower number density and a higher temperature being required at 143 km compared to those at 90 km. HCN and HC_3N vapor abundances were obtained from Coustenis et al. (2007).

We used six methane rotation lines between 70 and 165 cm^{-1} [R(6)–R(9); R(11)–R(12)] to determine a weighted average methane mole fraction at 70°N. R(10) is omitted due to contamination of the spectrum by a noise spike intrinsic to the CIRS instrument. Methane line lists were taken from Boudon et al. (2010), which are 0.883 times the HITRAN 2008 (Rothman et al., 2009) intensities and 1.019 times those of HITRAN 2004 (Rothman et al., 2005).

The strength of each methane rotation line was determined relative to the continuum. A best fit for $q(CH_4)$ was then obtained separately for each rotation line by minimizing χ^2. The strength for each line was weighted by a multiplier proportional to $\partial^2\chi^2/\partial q^2$, evaluated at $\chi^2 = \chi^2_{min}$; a final fit for the mole fraction was determined from the weighted average.

3.4. $q(CH_4)$ results at 70°N

Radiative transfer model fits to the CIRS methane rotation line spectrum at 70°N are shown in Fig. 4. Blow-ups of the individual lines are indicated in Fig. 5. The upper spectrum in Fig. 4 shows our best fit for a methane mole fraction $q(CH_4) = 1.50 \pm 0.15\%$ using the 74.1°N RSS temperature profile. The lower spectrum in Fig. 4 is for $q(CH_4) = 0.98 \pm 0.22\%$ (as derived by Lellouch et al., 2014, from CIRS limb integration data), in which we ran a forward model that incorporated the same RSS temperature structure as above, adjusted for the modified mean molecular mass. The latter fit clearly indicates that a value higher than $q(CH_4) = 0.98\%$ is needed (see also Fig. 5).

In addition to their limb integration determination, Lellouch et al. (2014) also derived a value $q(CH_4) = 1.24 \pm 0.14\%$ using CIRS nadir data at 70°N. A weighted average between their limb integration and nadir data retrievals yielded a value $q(CH_4) = 1.17 \pm 0.12\%$. They finally settled on a value of $q(CH_4) = 1.08 \pm 0.21\%$ after applying estimated corrections for *a priori* temperature errors. Comparing the Lellouch et al. (2014) value of 1.08 ± 0.21% to our derived mean mole fraction value of 1.50 ± 0.15% demonstrates the critical nature of adopting the RSS temperature profile. As we have shown in Fig. 2, it is extremely difficult to estimate *a priori* temperature structures in the methane rotation line formation altitude region from CIRS spectra at winter polar latitudes. The secondary temperature minimum at ~8–9 mbar in the RSS temperature profile at 74.1°N is almost impossible to anticipate, and yet its inclusion is crucial to the determination of $q(CH_4)$ at 70°N.

Lellouch et al. (2014) also inferred a value $q(CH_4) = 1.49 \pm 0.16\%$ at 62°N. A CIRS-independent determination of temperature structure at 62°N does not exist to compare with the one that Lellouch et al. (2014) derived from CIRS spectra, so we do not have an independent means of checking their methane mole fraction

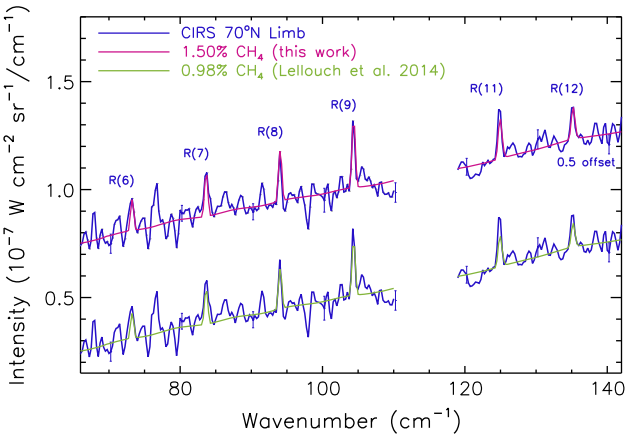

Fig. 4. CIRS limb spectra at latitude 70°N (blue curves) with a 0.5 offset in intensity units for the top spectrum. The average observed spectrum contains 25 spectra ranging in tangent height from 133 to 161 km. Six rotation methane lines [R(6)–R(9), R(11)–R(12)] were used in the analysis. The pink top curve is the best synthetic fit for a stratospheric methane mole fraction of 1.50 ± 0.15% at 70°N, using the RSS temperature profile at 74.1°N (temperature and pressure calculations assume a CH_4 mole fraction of 1.50%; see Schinder et al., 2012). The green bottom curve is a synthetic spectrum produced from the same radiative transfer model and essentially the temperature structure as the pink curve (see text for temperature adjustment), except the Lellouch et al. (2014) best fit mole fraction of 0.98% is adopted. (For interpretation of the references to color in this figure legend, the reader is referred to the web version of this article.)

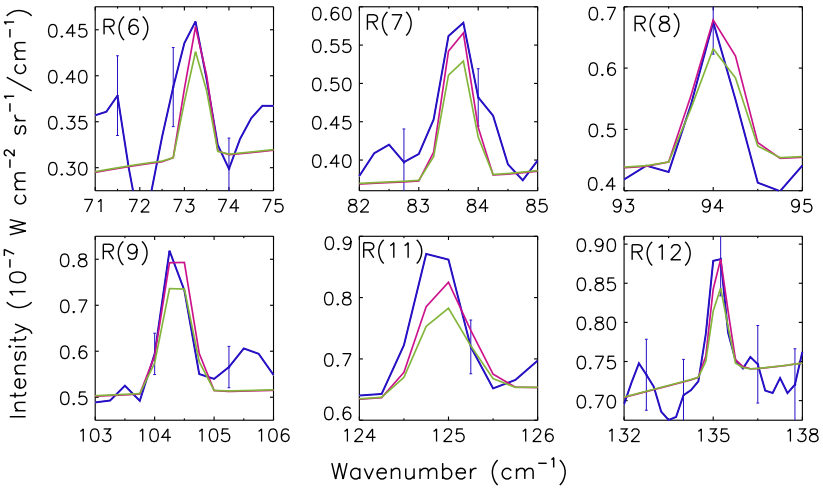

Fig. 5. Blow-ups of the six rotation methane lines used in the 70°N analysis. Color-coding is the same as in Fig. 4. (For interpretation of the references to color in this figure legend, the reader is referred to the web version of this article.)

value. However, their derived value is almost identical to our determined value of 1.50% at 70°N. We therefore adopt q(CH_4) = 1.50% as the stratospheric methane mole fraction at winter polar latitudes.

4. CIRS tropopause temperature retrieval at 85°N

Radiative transfer analyses of CIRS far-IR limb scan spectra at 85°N are used to infer a temperature profile in the region surrounding the tropopause at this latitude. Details of the retrieval procedure can be found in Anderson and Samuelson (2011). Just as the 1306 cm^{-1} ν_4 band of methane is the primary opacity source for deducing thermal structure from CIRS spectra between altitudes of ~160 km and 500 km (Achterberg et al., 2008), N_2–N_2 CIA in the spectral region between 70 and 140 cm^{-1} is the primary opacity source for the altitude region surrounding Titan's tropopause (ranging between about 30 and 200 mbar, although Lellouch et al., 2014, indicate a range 50 to 300 mbar). However, as discussed in Section 3.3 and shown in Fig. 3, additional contributions from the aerosol and stratospheric nitrile ice cloud must be included in the analysis.

We begin with an initial estimate of Titan's temperature profile from far-IR limb scan data at 85°N, and then use these scans to retrieve aerosol and ice opacities (both vertically and spectrally). Once the wavenumber and vertical dependence of aerosol and ice opacities are established, we apply a non-linear least squares *Levenberg–Marquardt* fitting technique to the CIRS spectra, coupled with our linearly constrained temperature inversion algorithm (Achterberg et al., 2008), to infer the temperature structure in the region surrounding the tropopause. We then systematically adjust the temperature profile through a range of temperature minima, each time readjusting the aerosol and ice opacities by using the *Levenberg–Marquardt* procedure. The final temperature profile between 30 and 200 mbar is the one for which χ^2 is a minimum at the tropopause. Formal 1σ uncertainties are roughly 0.5 K.

Fig. 6 depicts the 85°N limb integration spectrum with the synthetic fit superimposed that includes contributions from gaseous HCN, CO, CH_4, C_4H_2, C_2N_2, C_3H_4, HC_3N, and the Haystack. The HCN, HC_3N, and C_2N_2 vapor vertical abundance profiles are patterned after Teanby et al. (2006, 2007), the C_4H_2 and C_3H_4 profiles are taken from Vinatier et al. (2007), and CO was held uniform at 50 ppm. The quality of fit to the continuum implies the temperature profile retrieval between 30 and 200 mbar at 85°N is substantially correct. On the other hand, the temperature structure around

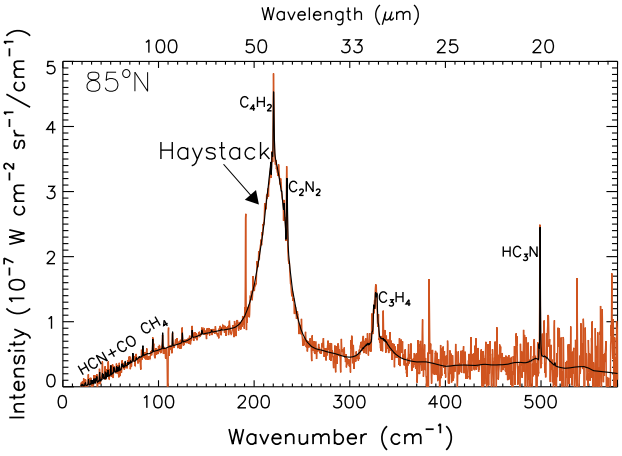

Fig. 6. 85°N far-IR limb integration (spectral resolution = 0.48 cm^{-1}) at an average tangent height of 136 km. Gases are labeled, as is the Haystack (broad ice emission feature peaking at 220 cm^{-1}). The data are shown in orange and the model fit is indicated by the black solid curve. Noise spikes are evident at ~110, 191.25, 383.0, 538.0, and 574.0 cm^{-1}. (For interpretation of the references to colour in this figure legend, the reader is referred to the web version of this article.)

the methane rotation line formation region, as determined from CIRS spectra, is intrinsically of very low quality (see Fig. 2 and the related discussion). Therefore the apparently good fit to the methane rotation lines observed between 60 and 100 cm^{-1} in Fig. 6 is logically largely fortuitous.

5. Results

Four temperature structures around the tropopause region are displayed in Fig. 7. The two at 53°N and 74°N were inferred from RSS data (Schinder et al., 2012), the one at 10°S from HASI (Fulchignoni et al., 2005), and the one at 85°N from the present study. Superimposed are four saturation vapor pressure curves. The short dash black, green, and gray curves were derived from the vapor-to-solid methane saturation vapor pressure law of Armstrong et al. (1955) for methane mole fractions of 0.62%, 1.09%, and 1.50%, respectively. The long dash gray curve is the ethane saturation vapor pressure (Lara et al., 1996) for a 0.0025% volume mixing ratio as determined by CIRS (Vinatier et al., 2007). Any portions of the temperature curves that fall to the left

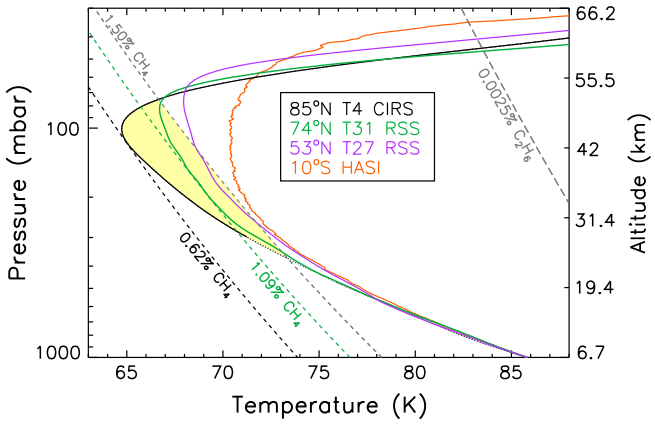

Fig. 7. Titan temperature profiles at 4 latitudes (solid curves) during mid northern winter from CIRS, RSS, and HASI. The dotted black curve at 85°N below the 300 mbar level is an extrapolation; it covers a pressure range where direct temperature information from CIRS is unavailable. Superimposed are saturation vapor pressure curves for 0.62%, 1.09% and 1.50% methane mole fractions (black dashed curve, green dashed curve, and short dash gray curve, respectively) and a 0.0025% ethane volume mixing ratio (long dash gray curve). Condensed methane should exist at altitudes where the temperature profile falls to the left of the 1.50% saturation vapor pressure curve (yellow highlighted area). Pressure–altitude relation is for 85°N only. (For interpretation of the references to color in this figure legend, the reader is referred to the web version of this article.)

of the saturation vapor pressure curves (area is highlighted in yellow for methane) are in altitude regions where some ethane and methane are in a solid phase. The figure indicates that some condensation of methane will occur at 85°N with a mole fraction $q(CH_4) > 0.62\%$, and at 74°N if $q(CH_4)$ is >1.09%.

As an aside, theoretical and laboratory work have shown that dissolving molecular nitrogen in liquid methane reduces the methane partial pressure by ~20% (Thompson et al., 1992). A 20% reduction in the methane partial pressure will reduce the stratospheric vapor mole fraction from 1.50% to 1.20%, which is still significantly higher than the 0.62% necessary to induce methane condensation in Titan's stratosphere at 85°N. On the other hand, due to the very cold temperatures at altitudes surrounding Titan's tropopause at 85°N and 74°N, methane converts directly from the vapor to the solid phase, making it more difficult to incorporate N_2 into the condensate. We suspect the amount of molecular nitrogen dissolved in the molecular N_2–CH_4 ice mixture may be considerably less than 20%.

It is clear from Fig. 7 that methane condensation through subsidence in Titan's lower stratosphere/upper troposphere is unavoidable poleward of ~74°N, and the associated SIMCs will form upper boundaries in the lower stratosphere near 50 km at 85°N and at the tropopause near 48 km at 74°N, assuming a methane mole fraction of 1.50%. Very little if any condensation is likely to occur between 53°N and 10°S, and only in the troposphere. Note that for latitudes poleward of ~74°N, condensation due to subsidence will occur at considerably higher altitudes than will condensation due to convection at low latitudes. The pressure-altitude relation plotted in Fig. 7 is for 85°N only.

Let ΔT be the temperature difference at a given altitude between Titan's atmospheric temperature T(atm) (indicated by the solid curves in Fig. 7) and the methane condensation temperature T(sat) for $q(CH_4) = 1.50\%$ (shown by the short dash gray curve in Fig. 7). We define ΔT_{min} to be the value of ΔT where the difference [T(atm)–T(sat)] is most negative (or least positive); these differences are illustrated in Fig. 8b. During northern winter, large negative differences in ΔT_{min} are observed near both poles, whereas small ΔT_{min} (less negative or even positive) values are observed at low and mid latitudes. The smaller values of $q(CH_4)$ at low latitudes inferred from CIRS data by Lellouch et al. (2014) favor positive values of ΔT_{min} there. At high southern latitudes during northern winter, insolation is strong at the surface, and this can lead to atmospheric instability that may trigger convection in the troposphere. During this time of year, methane cumulus clouds were consistently observed in the troposphere, most likely due to convection induced by surface heating (see for example Roe et al., 2002). Hence, the large negative differences in ΔT_{min} at these high southern latitudes most likely reflect convection-induced formation processes that dominate over those due to general circulation.

Unlike methane, the temperature difference ΔT_{min} for ethane is always a large negative number regardless of latitude and time of year, leading to the generally uniform appearance of Titan's northern polar ethane cloud structure as observed by VIMS (Griffith et al., 2006; Le Mouélic et al., 2012; Rannou et al., 2012). Diffuse ethane clouds have been observed near the north winter pole and not at lower latitudes because strong subsidence occurs in the polar region during winter. Some condensation of ethane most likely occurs at low latitudes in the stratosphere but the resulting steady-state cloud formation is optically too thin to be observed. Since Titan's tropopause temperature is always far from the ethane condensation temperature (Fig. 7), any slight temperature

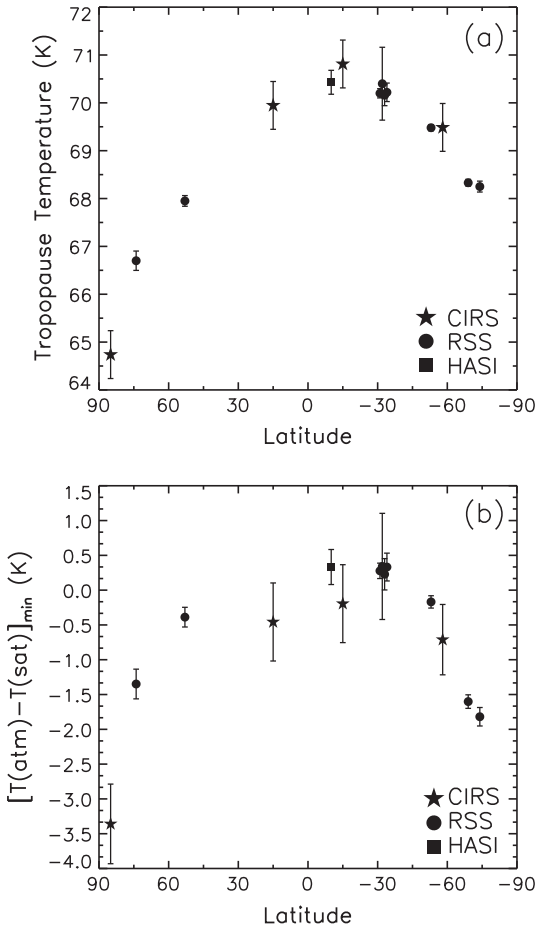

Fig. 8. (a) Latitude variation of tropopause temperatures during northern winter with 1σ uncertainties determined from CIRS (black filled stars), RSS (black filled circles), and HASI (black filled square). (b) Latitude variation of the minimum difference between Titan's temperature and the methane condensation temperature (ΔT_{min}) for CIRS (stars), RSS (circles), and HASI (square). A 1.50% CH_4 mole fraction is adopted throughout. Large negative differences seen near the poles and absent at low and mid latitudes are indicative of methane being in the solid phase in Titan's lower stratosphere/upper troposphere at high latitudes.

perturbations from dynamically-induced processes such as waves, wind shears, and horizontal advection, will not cause large departures from homogenous cloud structures. For methane, on the other hand, small temperature fluctuations (Figs. 7 and 8b) can have significant effects on the ice abundance, and hence on the optical thickness. Thus, we would expect Titan's methane cloud structure to appear heterogeneous, independently of the formation mechanism, whether convection- or subsidence-induced.

As an aside, both convection- and subsidence-induced methane clouds will always have cloud upper boundaries at lower altitudes than companion ethane clouds. This can be seen in Fig. 7 by the altitude location where the methane and ethane saturation vapor pressure curves intersect Titan's temperature structures. Note also that at some latitudes subsidence-induced methane clouds lie entirely in the upper troposphere. Thus cloud altitude and/or morphology alone do not by themselves demonstrate that methane clouds are convective.

6. VIMS example of SIMCs

Titan's north polar cloud system was initially discovered by VIMS in December 2004 (Griffith et al., 2006). It was observed to span latitudes 51°N to the terminator at 68°N during early-to-mid northern winter on Titan when all latitudes poleward of 68°N were in polar shadow. Griffith et al. (2006) applied radiative transfer analyses of spectra at latitudes 48°N to 55°N and inferred cloud altitudes between 30 and 60 km; these low altitudes effectively ruled out condensates other than ethane and methane. These same analyses by Griffith et al. (2006) also indicated that effective cloud particle radii could not exceed ~3 μm, since there was no evidence of cloud opacity in the VIMS 5 μm spectra. This, coupled with the extensive, long-lasting, and homogeneous nature of the cloud system, implied that at least a substantial fraction of the condensate was contained in Titan's lower stratosphere, and that it was probably comprised of condensed ethane.

As Titan's northern winter progressed and the north polar latitudes were no longer in shadow, subsequent VIMS analyses spanning the time period from late 2006 through 2007 indicated that two types of cloud morphology comprising the vast north polar cloud system had emerged (Rannou et al., 2012; Le Mouélic et al., 2012). The first morphological type was most likely due to ethane ice, with a diffuse, homogeneous appearance that extended from ~55°N to the pole. This was the cloud system that Griffith et al. (2006) had initially observed. The second morphological type displayed heterogeneous horizontal structure poleward of ~64°N. This is the type of cloud system that we attribute to SIMCs. An example is the copper-colored cloud system visible at latitudes poleward of 64°N in the VIMS T22 (December 2006) image depicted in Fig. 9. This cloud system is readily observed at 5 μm, suggesting particle cross sections associated with particle radii considerably larger than those proposed for ethane clouds (1–3 μm radii) by Griffith et al. (2006). On the other hand, the amount of methane available for condensation is about 200 times greater than that of ethane. This leads to methane ice particle mean radii about 6 times greater than those for ethane ice, large enough to be readily observable at 5 μm. Radiative transfer analyses of these VIMS data in the latitude range ~70°N to 73°N place the cloud tops near 55 km with maximum optical thicknesses ~35 (Rannou et al., 2012). Large uncertainties are associated with both parameters. However, the two parameters are anticorrelated – the smaller the optical thickness, the higher the cloud top, and vice versa. In spite of the large uncertainties, it appears that these clouds are most likely both thick and high. Since methane is ~200 times more abundant than ethane, such large optical thicknesses are compatible with those expected for methane clouds but not for the much more homogeneous and optically thinner ethane ice component of the north polar cloud system. The relatively high cloud top altitudes appear to favor SIMCs over convection-induced methane clouds.

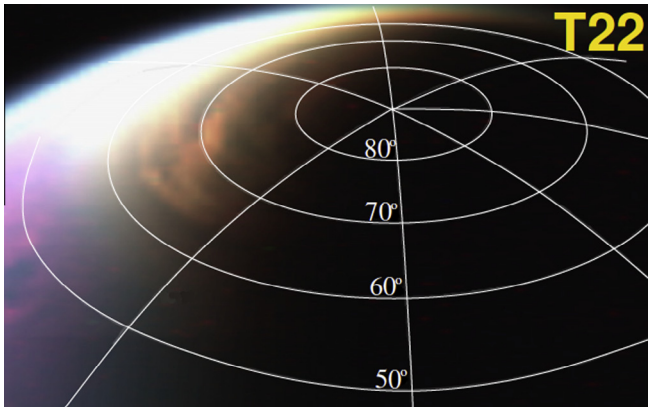

Fig. 9. VIMS color composite image of the north polar cloud system recorded on 22 December 2006. Red = 5 μm, green = 2.78 μm, and blue = 2.03 μm; adapted from Fig. 1c in Le Mouélic et al. (2012). Superimposed (white curves) are grids spaced every 10° in latitude and 45° in longitude. Two types of cloud morphologies are apparent. The first is associated with a homogeneous diffuse cloud system that extends poleward of ~53°N; this is most likely due to condensed ethane (see Griffith et al., 2006). The second (copper colored) cloud system is seen at 5 μm, and has an inhomogeneous morphology that extends poleward of 64°N; this cloud system most likely is composed of condensed methane. (For interpretation of the references to color in this figure legend, the reader is referred to the web version of this article.)

Possible contributors to Titan's late winter/early spring high latitude methane clouds may be lake-effect clouds triggered by convection (Brown et al., 2009). This type of cloud has a somewhat streaked morphology due to wind shear and may be less optically thick and lower in altitude than the 5 μm bright optically thick heterogeneous clouds seen in the VIMS T22 image near the pole (Fig. 9). These putative lake-effect clouds have been observed by both VIMS (Brown et al., 2009) and by the Imaging Science Subsystem (ISS), with the latter observations at latitudes 60°N to 80°N (Turtle et al., 2011) and close to northern spring equinox. One might expect to see lake-effect convective methane clouds (if that is what they are) near spring equinox when sunlight at the surface at high northern latitudes can trigger convection.

One point must be emphasized, however: Figs. 7 and 8b demonstrate that Titan's SIMCs must almost inevitably form at near-polar latitudes during winter, no matter what else may be occurring at that time. During early northern spring, it may be very difficult to distinguish between convection-induced methane clouds and SIMCs at mid latitudes. At these latitudes, both types of methane clouds will have relatively low cloud tops, will be highly heterogeneous, and will have particle radii as large as a few tens of microns (Griffith et al., 2006, 2009; Rannou et al., 2006, 2012; Brown et al., 2009).

7. Synopsis and discussion

A large cloud system in Titan's north polar region was observed in reflected sunlight at 5 μm from a VIMS image acquired on 22 December 2006. This was during Titan's mid winter season (Fig. 9). The system extended from ~64°N to ~74°N, above which it was in polar shadow. Radiative transfer analyses by Rannou et al. (2012) suggested a cloud top near 55 km with a cloud optical thickness ~35 where the cloud was densest. Intense reflected solar radiation from clouds at 5 μm implies particle radii >10 μm or so, while a large optical thickness requires cloud abundances

considerably greater than could be provided by trace volatiles such as ethane. Both conditions strongly suggest methane ice as the only viable candidate for the cloud composition. A cloud top at 55 km is roughly consistent with the cloud top level that we predict for a Subsidence-Induced Methane Cloud.

Dry GCMs predict a slow, axisymmetric meridional circulation pattern, with flow from summer to winter poles in the stratosphere and mesosphere, and a return flow in the troposphere (e.g. Hourdin et al., 1995). Thus, during northern winter, methane vapor will originate from the surface, enter the stratosphere mainly at southern high latitudes, cross the equator, and descend at high northern latitudes. Because the vertical temperature gradient is mostly positive in the stratosphere, methane will descend from warmer regions into colder ones at high winter latitudes and partially condense in the lower stratosphere, provided the methane mole fraction is high enough and the temperature is cold enough for saturation to occur.

We tested these requirements with radiative transfer analyses of CIRS data acquired at high northern (winter) latitudes. Both CIRS limb-tangent spectra and RSS radio occultation temperature profiles were utilized in the analyses. A stratospheric methane mole fraction of q(CH_4) ~1.50% was inferred at latitudes ~70–74°N. Tropopause temperatures were found to decrease steadily from low latitudes to 85°N (Figs. 7 and 8a).

We assumed that the derived value of q(CH_4) ~1.50% is representative of stratospheric methane mole fractions throughout the northern high latitude region during northern winter. Based on the temperature profiles derived at different latitudes in the general region around the tropopause, we infer that methane clouds will begin to form northward of somewhere between 53°N and 74°N (see Fig. 7). This is consistent with a southern cloud boundary at ~64°N, as indicated by the VIMS image shown in Fig. 9. According to Fig. 7, most condensation will occur in the upper troposphere, but some condensation will also occur in the lower stratosphere at latitudes somewhere above 74°N. This is reasonably consistent with cloud altitudes of ~55 km between 70–73°N as determined by Rannou et al. (2012), in view of the large uncertainties associated with the various analyses.

We believe a strong, internally consistent case now exists for the presence of SIMCs in the lower stratosphere/upper troposphere at high winter latitudes on Titan. Convective methane clouds at these latitudes seem unlikely under polar winter conditions because incident sunlight is at most very weak at Titan's surface, and thermally induced dynamic instabilities at the surface are minimal. Thus, in the presence of subsidence, the lapse rate in Titan's winter troposphere is unlikely to exceed the adiabatic lapse rate (wet or dry).

A few aspects of the overall picture remain unclear. It has been thought for some time that the methane mole fraction in Titan's stratosphere should be more or less constant, independent of latitude (see e.g. Dire, 2000). The value of q(CH_4) ~1.48% inferred from GCMS (Niemann et al., 2010) at 10°S was thought to determine this amount. The recent study by Lellouch et al. (2014), however, has made the picture more complex. Using both CIRS nadir and limb-tangent data, they attempt to derive simultaneously both vertical temperature profiles and stratospheric methane mole fractions as functions of latitude. Considering only winter data prior to March 2008, Lellouch et al. (2014) infer low values for the methane mole fraction at low latitudes [q(CH_4) ~1.0% at 15°S, 0°, and 15°N] and high values at high latitudes [q(CH_4) ~1.5% at 80°S and 62°N]. The exception [q(CH_4) ~1.1% at 70°N] is the one we adjust to q(CH_4) ~1.50%, as discussed in Section 3.

The simple single-cell circulation model seems consistent with the idea that the methane mole fraction would remain roughly constant along stream lines as methane was transported from high southern latitudes in the stratosphere to high northern latitudes (see Fig. 1). On the other hand, we would not expect an amount of methane vapor compatible with q(CH_4) ~1.55% (the value inferred by Lellouch et al., 2014) to be able to pass upward through the cold trap at 80°S (see Fig. 8b). Condensation would limit the final mole fraction to a lesser amount.

Lellouch et al. (2014) suggest a possible mechanism for transporting excess methane through the cold trap. They derive somewhat higher values for stratospheric q(CH_4) at certain intermediate latitudes compared with values at adjacent locations. They note that the former are latitudes at which clouds have been seen, and propose these latitudes may be associated with regions in which convective overshoot occurs. Noting that Griffith et al. (2005) reported upwelling cloud velocities of 2–10 m s^{-1}, Lellouch et al. (2014) suggest that methane cloud particles might undergo convective penetration of the cold trap and subsequently evaporate, thereby enhancing the value of q(CH_4) in the warmer local stratosphere above.

Though highly speculative, the same process may have occurred near 80°S. A relatively dense network of convective cloud cells was observed by ISS in the vicinity of the southern polar region between 3 July 2004 and 6 June 2005 (Turtle et al., 2009). Intense insolation at the surface at this time might have caused strong convective updrafts, resulting in cloud particle penetration of the cold trap with concomitant buildup, through evaporation, of excess methane vapor in the lower stratosphere until a value q(CH_4) ~1.5% was reached. Meridional circulation would then have transported this mole fraction to high northern latitudes, where subsidence would give rise to SIMCs.

We conclude that, although there is some flexibility in the exact amount of methane ice contained in the polar cloud during northern winter, it is almost inevitable that methane dominates the cloud composition at the most extreme northern latitudes, and that subsidence is the physical transport process responsible for cloud formation there.

Acknowledgments

The authors acknowledge funding support from NASA's Cassini Project and NASA's Cassini Data Analysis and Participating Scientist program.

References

Achterberg, R.K., Conrath, B.J., Gierasch, P.J., Flasar, F.M., Nixon, C.A., 2008. Titan's middle-atmospheric temperatures and dynamics observed by the Cassini Composite Infrared Spectrometer. Icarus 194, 263–277.

Anderson, C.M., Samuelson, R.E., 2011. Titan's aerosol and stratospheric ice opacities between 18 and 500 μm: Vertical and spectral characteristics from Cassini CIRS. Icarus 212, 762–778.

Anderson, C.M., Samuelson, R.E., Bjoraker, G.L., Achterberg, R.K., 2010. Particle size and abundance of HC_3N ice in Titan's lower stratosphere at high northern latitudes. Icarus 207, 914–922.

Armstrong, G.T., Brickwedde, F.G., Scott, R.B., 1955. Vapor pressures of the methanes. J. Res. Nat. Bureau Stand. 55, 39–53.

Borysow, A., Frommhold, L., 1986a. Collision-induced rototranslational absorption spectra of N_2–N_2 pairs for temperatures from 50 to 300 K. Astrophys. J. 311, 1043–1057.

Borysow, A., Frommhold, L., 1986b. Theoretical collision-induced rototranslational absorption spectra for modeling Titan's atmosphere - H_2–N_2 pairs. Astrophys. J. 303, 495–510.

Borysow, A., Frommhold, L., 1986c. Theoretical collision-induced rototranslational absorption spectra for the outer planets – H_2–CH_4 pairs. Astrophys. J. 304, 849–865.

Borysow, A., Tang, C., 1993. Far Infrared CIA Spectra of N_2–CH_4 pairs for modeling of Titan's atmosphere. Icarus 105, 175–183.

Boudon, V., Pirali, O., Roy, P., Brubach, J.B., Manceron, L., Vander Auwera, J., 2010. The high-resolution far-infrared spectrum of methane at the SOLEIL synchrotron. J. Quant. Spectro. Rad. Trans. 111, 1117–1129.

Brown, M.E. et al., 2009. Discovery of lake-effect clouds on Titan. Geophys. Res. Lett. 36, 1103.

Coustenis, A., Achterberg, R.K., Conrath, B.J., Jennings, D.E., Marten, A., Gautier, D., Nixon, C.A., Flasar, F.M., Teanby, N.A., Bézard, B., Samuelson, R.E., Carlson, R.C., Lellouch, E., Bjoraker, G.L., Romani, P.N., Taylor, F.W., Irwin, P.G., Fouchet, T.,

Hubert, A., Orton, G.S., Kunde, V.G., Vinatier, S., Mondellini, J., Abbas, M.M., Courtin, R., 2007. The composition of Titan's stratosphere from Cassini/CIRS mid-infrared spectra. Icarus 189, 35–62.
Dire, J.R., 2000. Seasonal photochemical and meridional transport model for the stratosphere of Titan. Icarus 145, 428–444.
Fjeldbo, G., Eshleman, V.R., 1968. The atmosphere of Mars analyzed by integral inversion of the Mariner IV occultation data. Planet. Space Sci. 16, 1035–1059.
Flasar, F.M., 1983. Oceans on Titan? Science 221, 55–57.
Flasar, F.M., Samuelson, R.E., Conrath, B.J., 1981. Titan's atmosphere – Temperature and dynamics. Nature 292, 693–698.
Fulchignoni, M. et al., 2005. In situ measurements of the physical characteristics of Titan's environment. Nature 438, 785–791.
Griffith, C.A. et al., 2005. The evolution of Titan's mid-latitude clouds. Science 310, 474–477.
Griffith, C.A. et al., 2006. Evidence for a polar ethane cloud on Titan. Science 313, 1620–1622.
Griffith, C.A. et al., 2009. Characterization of clouds in Titan's tropical atmosphere. Astrophys. J. 702, L105–L109.
Hourdin, F., Talagrand, O., Sadourny, R., Courtin, R., Gautier, D., McKay, C.P., 1995. Numerical simulation of the general circulation of the atmosphere of Titan. Icarus 117, 358–374.
Khanna, R., Pererajarmer, M., Ospina, M., 1987. Vibrational infrared and Raman spectra of dicyanoacetylene. Spectrochim. Acta Part A: Mol. Spectrosc. 43, 421–425.
Lara, L.M., Lellouch, E., López-Moreno, J.J., Rodrigo, R., 1996. Vertical distribution of Titan's atmospheric neutral constituents. J. Geophys. Res. 101, 23261–23283.
Le Mouélic, S. et al., 2012. Dissipation of Titan's north polar cloud at northern spring equinox. Planet. Space Sci. 60.
Lebonnois, S., Burgalat, J., Rannou, P., Charnay, B., 2012. Titan global climate model: A new 3-dimensional version of the IPSL Titan GCM. Icarus 218, 707–722.
Lellouch, E., Bezard, B., Flasar, F.M., Achterberg, R., Nixon, C.A., Bjoraker, G.L., Gorius, N., 2014. The distribution of methane in Titan's stratosphere from Cassini/CIRS observations. Icarus 231, 323–337.
Leovy, C.B., Pollack, J.B., 1973. A first look at atmospheric dynamics and temperature variations on Titan. Icarus 19, 195–201.
Mayo, L.A., Samuelson, R.E., 2005. Condensate clouds in Titan's north polar stratosphere. Icarus 176, 316–330.
Niemann, H.B. et al., 2010. Composition of Titan's lower atmosphere and simple surface volatiles as measured by the Cassini-Huygens probe gas chromatograph mass spectrometer experiment. J. Geophys. Res. (Planets) 115, 12006.
Porco, C.C. et al., 2005. Imaging of Titan from the Cassini spacecraft. Nature 434, 159–168.
Rannou, P., Montmessin, F., Hourdin, F., Lebonnois, S., 2006. The latitudinal distribution of clouds on Titan. Science 311, 201–205.
Rannou, P., Le Mouélic, S., Sotin, C., Brown, R.H., 2012. Cloud and Haze in the winter polar region of Titan observed with visual and infrared mapping spectrometer on board Cassini. Astrophys. J. 748, 6 (Article id: 4).
Rodriguez, S., Le Mouélic, S., Rannou, P., Sotin, C., Brown, R.H., Barnes, J.W., Griffith, C.A., Burgalat, J., Baines, K.H., Buratti, B.J., Clark, R.N., Nicholson, P.D., 2011. Titan's cloud seasonal activity from winter to spring with Cassini/VIMS. Icarus 216, 89–110.
Roe, H.G., de Pater, I., Macintosh, B.A., McKay, C.P., 2002. Titan's clouds from Gemini and Keck adaptive optics imaging. Astrophys. J. 581, 1399–1406.
Rothman, L.S. et al., 2005. The HITRAN 2004 molecular spectroscopic database. J. Quant. Spectro. Rad. Trans. 96, 139–204.
Rothman, L.S. et al., 2009. The HITRAN 2008 molecular spectroscopic database. J. Quant. Spectro. Rad. Trans. 110, 533–572.
Samuelson, R.E., Mayo, L.A., Knuckles, M.A., Khanna, R.J., 1997a. C_4N_2 ice in Titan's north polar stratosphere. Planet. Space Sci. 45, 941–948.
Samuelson, R.E., Nath, N.R., Borysow, A., 1997b. Gaseous abundances and methane supersaturation in Titan's troposphere. Planet. Space Sci. 45, 959–980.
Samuelson, R.E., Smith, M.D., Achterberg, R.K., Pearl, J.C., 2007. Cassini CIRS update on stratospheric ices at Titan's winter pole. Icarus 189, 63–71.
Schinder, P.J. et al., 2011. The structure of Titan's atmosphere from Cassini radio occultations. Icarus 215, 460–474.
Schinder, P.J., Flasar, F.M., Marouf, E.A., French, R.G., McGhee, C.A., Kliore, A.J., Rappaport, N.J., Barbinis, E., Fleischman, D., Anabtawi, A., 2012. The structure of Titan's atmosphere from Cassini radio occultations: Occultations from the prime and equinox missions. Icarus 221, 1020–1031.
Teanby, N.A., Irwin, P.G.J., de Kok, R., Nixon, C.A., Coustenis, A., Bézard, B., Calcutt, S.B., Bowles, N.E., Flasar, F.M., Fletcher, L., Howett, C., Taylor, F.W., 2006. Latitudinal variations of HCN, HC_3N, and C_2N_2 in Titan's stratosphere derived from Cassini CIRS data. Icarus 181, 243–255.
Teanby, N.A., Irwin, P.G.J., de Kok, R., Vinatier, S., Bézard, B., Nixon, C.A., Flasar, F.M., Calcutt, S.B., Bowles, N.E., Fletcher, L., Howett, C., Taylor, F.W., 2007. Vertical profiles of HCN, HC_3N, and C_2H_2 in Titan's atmosphere derived from Cassini/CIRS data. Icarus 186, 364–384.
Thompson, W.R., Zollweg, J.A., Gabis, D.H., 1992. Vapor–liquid equilibrium thermodynamics of $N_2 + CH_4$ – Model and Titan applications. Icarus 97, 187–199.
Turtle, E.P. et al., 2009. Cassini imaging of Titan's high-latitude lakes, clouds, and south-polar surface changes. Geophys. Res. Lett. 36, 2204.
Turtle, E.P. et al., 2011. Seasonal changes in Titan's meteorology. Geophys. Res. Lett. 38, 3203.
Vinatier, S., Bézard, B., Fouchet, T., Teanby, N.A., de Kok, R., Irwin, P.G.J., Conrath, B.J., Nixon, C.A., Romani, P.N., Flasar, F.M., Coustenis, A., 2007. Vertical abundance profiles of hydrocarbons in Titan's atmosphere at 15°S and 80°N retrieved from Cassini/CIRS spectra. Icarus 188, 120–138.